IEEE Photonics Journal
An IEEE Photonics Society Publication

Open Access

A Pixilated Spectrometer Based on Single Liquid Crystal and Sparse Algorithm

Volume 8, Number 5, October 2016

Feiying Sun
Liangping Xia
Zheng Yang
Jun Cui
Ziyin Zhang
Chang bin Nie
Danjun Liu
Shaoyun Yin
Guoxing Zheng
Peng Wu
Ruofu Yang
Chunlei Du

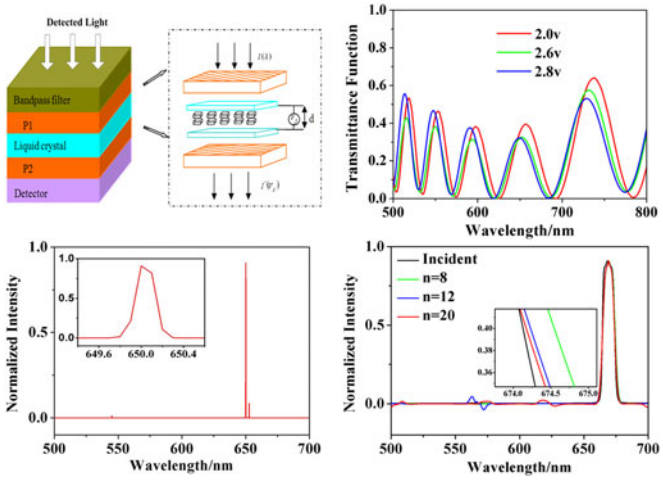

DOI: 10.1109/JPHOT.2016.2597190
1943-0655

A Pixilated Spectrometer Based on Single Liquid Crystal and Sparse Algorithm

Feiying Sun,[1] Liangping Xia,[1] Zheng Yang,[1] Jun Cui,[1,2] Ziyin Zhang,[1] Chang bin Nie,[1] Danjun Liu,[1] Shaoyun Yin,[1] Guoxing Zheng,[1,2] Peng Wu,[1] Ruofu Yang,[1] and Chunlei Du[1]

[1]Chongqing Key Laboratory of Multi-scale Manufacturing Technology, Chongqing Institute of Green and Intelligent Technology, Chinese Academy of Sciences, Chongqing 400714, China
[2]School of Electronic Information, Wuhan University, Wuhan 430072, China

DOI:10.1109/JPHOT.2016.2597190

Manuscript received July 24, 2016; accepted July 28, 2016. Date of current version October 11, 2016. This work was supported in part by the National Science Foundation of China under Grant 61275061, Grant 11174281, Grant 61504147, Grant 61475199, and Grant 61308062; in part by the Application Development Project of Chongqing, China, under Grant cstc2013yykfC00007; in part by the Fundamental & Advanced Research Projects of Chongqing, China, under Grant cstc2013jcyjC00001; and in part by the Scientific Equipment Research Project of Chinese Academy of Sciences (Development of THz imaging spectrometer for biomacromolecules). Corresponding author: C. Du (e-mail: cldu@cigit.ac.cn).

Abstract: A method of achieving integrated microspectrometer with small size, high-energy efficiency, and high spectrum resolution is proposed. This spectrometer utilizes the single-pixilated liquid crystal (LC) and a matched sparse representation algorithm. The properties of compact size and high-energy efficiency are benefit to the configuration of single-pixilated LC which forms a filter array in the time domain for the polarization interference turned by driven voltage. The high spectrum resolution is obtained with the application of sparse representation of the nonnegative L1 minimization algorithm. By theoretical derivation, the physical model of the microspectrometer is set up, and the experimental results indicate the effectiveness of spectrum reconstruction with a spectrum resolution of about 0.2 nm.

Index Terms: Integrated optics devices, spectroscopy, high resolution, liquid crystals.

1. Introduction

With the development of integrated photonic devices, microspectrometer has blossomed into a research hotspot [1]. Several types of microspectrometer have been presented [2]–[9], [15], the micro-electromechanical systems [2] and the planar waveguide [3], [4], [15], for example. While the micro-electromechanical systems have a limitation of application due to its low resolution and the planar waveguide suffers from a narrow bandwidth and low optical efficiency. Recently, another kind of microspectrometer has been reported [5]–[8], including those based on the filter array with its related algorithm [5]–[7], which offers a novel method. However, the spectral energy of these spectrometers is equally distributed to each filter unit, which gives rise to a lower utilization rate of energy with more filter units. In addition, the integration of the filter array suffers from a certain spatial scale. The optimal way to resolve the problem of energy efficiency and space scale is to generate a filter array in only one unit. Liquid crystal (LC) as a single pixel unit is benefit for its excellent optical modulation ability [9]–[14] when the driven voltage is applied, which converts the scale of spatial-domain into time-domain. When the algorithm comes into incorporation to form a

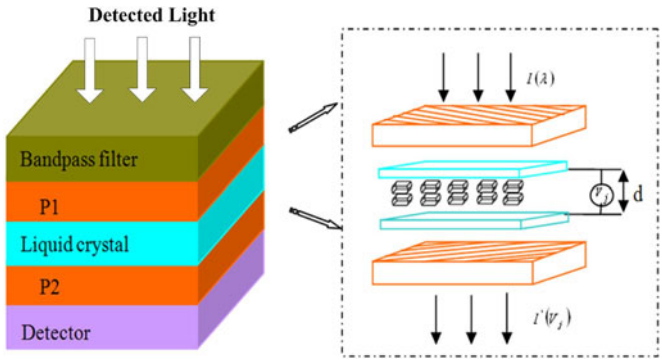

Fig. 1. Schematic diagram of the proposed pixelated spectrometer. Incident spectrum passing through the LC driven by the voltages makes the birefringence interference and changes the detected intensity.

microspectrometer, the energy utilization efficiency increases, and spatial scale tend to be further small. In this paper, we present a pixilated spectrometer based on the single LC and a sparse algorithm. Compared to the spectrometer of filter array, the pixilated spectrometer has the feasible design, making the high optical efficiencies and small size available. The feasibility of this method is verified by analysis of the theoretical model and experiment results.

2. Simulation

The configuration of the pixilated spectrometer is shown in Fig. 1. It contains layers of bandpass optical filter, polarizer 1 (P1), single birefringence LC with a pixel size of conducting layer, polarizer 2 (P2), and detector. The bandpass filter is used to choose the detection spectrum range. The layer of P1, LC and P2 constitute the filter with the birefringence interference. With the variation of driven voltage, the birefringence interference changes accordingly, and then, the transmitted light can be detected by the detector.

When the direction of polarizer P1 and P2 are orthogonal and the driven voltage is V_j, the intensity of the transmitted light from P2 is defined as [10], [11]

$$I'(V_j, \lambda_i) = I(\lambda_i)\sin^2 2\varphi \times \exp(-\alpha_0 d)\left(1 - \cos\frac{2\pi d\Delta n(V_j)}{\lambda_i}\right) = I(\lambda_i)t_{ij} \tag{1}$$

where λ_i is the wavelength of the incident light, α_o is the absorption coefficient of o-light, d is the thickness of the LC, $I(\lambda_i)$ is the incident intensity after passing the bandpass filter, and φ is the included angle between the transmitting direction of polarizer P1 and the direction of optical axis of LC, where Δn is the refractive index difference between the o-light and e-light and is decided by the drive voltage. By simplifying the formula, the modulation of the incident light can be written as t_{ij}, which is defined as the transmittance function.

Considering this formula (1), when the material of LC and its thickness is determined, the absorption coefficient α_o, φ and d are constant. The transmittance function t_{ij} is only related to the driven voltage V_j and the wavelength λ_i of the incident light. In this case, the transmittance function can be written as $t_{ij}(V_j, \lambda_i)$.

For the detector, the incident light of all wavelengths is detected. When the driven voltage is determined, the detected intensity is the sum at different wavelength. With (1), the intensity received by the detector [5] is

$$I'(V_j) = \int_\lambda I'(V_j, \lambda_i)d\lambda = \int_\lambda \mathrm{t_{ij}}(\mathrm{V_j}, \lambda_i)\mathrm{I}(\lambda_i)\,\mathrm{d}\lambda \tag{2}$$

By dispersing the wavelength of the incident light, the incident intensity can be written as a vector, which is $I = (I_1(\lambda_1), I_2(\lambda_2), ...I_m(\lambda_m))^T$. By dispersing the driven voltage, the detected intensity is

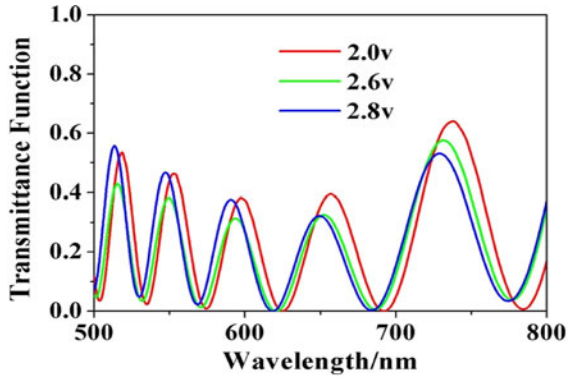

Fig. 2. Relationship of the transmittance function between the driven voltage and incident wavelength. Transmittance under the driven voltage: 2.0, 2.6, 2.8 V.

another vector $I' = (I'_1(V_1), I'_2(V_2), ...I'_n(V_n))^T$. With this method, (2) is equal to the following matrix equation:

$$\begin{bmatrix} I'_1 \\ I'_2 \\ .... \\ I'_n \end{bmatrix} = \begin{bmatrix} t_{11} & t_{22} & .... & t_{1m} \\ t_{21} & t_{22} & .... & t_{2m} \\ .... & .... & .... & .... \\ t_{n1} & t_{n2} & .... & t_{nm} \end{bmatrix} \begin{bmatrix} I_1 \\ I_2 \\ .... \\ I_m \end{bmatrix} \text{Or } I'_{n\times 1} = T_{n\times m} I_{m\times 1} \tag{3}$$

where $T_{n\times m}$ is a discrete transmission function.

For the pixilated spectrometer with single LC, I' is detected by the photoelectric detector and $T_{n\times m}$ is measured as shown in Fig. 2. Then, the spectrum of the incident light can be retrieved from (3). For the spectrometer, to get a high spectrum resolution requires to increase the sampling frequency in spectrum domains, which leads the element number m to be a big number. With regard to the polarization interference of LC, the different interference needs a large refractive index difference between the ordinary light and extraordinary light, which means that the discrete interval of the driven voltage have to be large enough. A conclusion can be draw that the element number n is much smaller than m. In this case, the spectrum of the incident light I cannot be solved directly by matrix inversion from (3).

To solve the spectrum of the incident light from (3), the method of sparse representation of signals is adopted. In this method, the incident light can be described as $I = \psi s$, where ψ is the sparse dictionary with a dimension of $m \times p (p > n)$ and s is the sparse signal with $p \times 1$ [12], [16], [17]. Hence, (3) can be rewritten as

$$I' = TI = T\psi s. \tag{4}$$

Considering that $A = T\psi$, a sparse signal recovery $\hat{s}$ can be solved with the mathematic method of non-negative L_1 minimization algorithm

$$\hat{s} = \min_s \|s\|_1 + \frac{\tau}{2} \left\| I' - A s \right\|_2^2 \text{ subject to } \quad s \geq 0 \tag{5}$$

where τ is regularization parameter to decide the weight of two parts of (5).

With the obtained sparse solution $\hat{s}$, the spectrum of the incident light can be solved:

$$I = \psi \hat{s}. \tag{6}$$

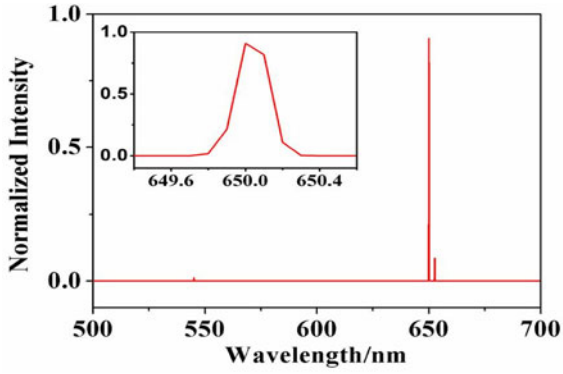

Fig. 3. Monochromatic spectra reconstruction of 650 nm. (Top left inset) Magnification of monochromatic spectrum.

In this sparse algorithm, the theory spectral resolution of the microspectrometer is defined as follows [12]:

$$\Delta\lambda = \mu_m \Delta\lambda_m = \mu_m \frac{W_\lambda}{m} \tag{7}$$

where W_λ is the responding spectral bandwidth of the light transmitted through the bandpass filter. $\Delta\lambda_m = \frac{W_\lambda}{m}$ is the discrete interval of the spectrum. μ_m is the integer of initial guess determined by the transmittance function and the sparse representation.

3. Experiment and Discussion

To verify the performance of the pixilated spectrometer, the transmittance function T is measured. The nematic birefringence LC with 22 μm thickness is chosen (S100A220UG180), and its transmittance function t_{ij} can be measured with the spectrophotometer Lambda 35. During the measurement process, the driven voltage applied on the LC is the alternating current (AC) square wave voltage with the duty cycle of 50% and the frequency of 1 kHz. The driven voltage varies from 1.0 to 4.0 V with an interval of 0.1 V. The wavelength ranges from 500 to 800 nm with an interval of 0.1 nm. The measurement result of the transmission spectrum is shown in Fig. 2, which indicates that the used LC suffers from low quality factor, and the birefringence interference is periodic. Apparently, the spectrum of incident light cannot be achieved directly by the interference of LC.

In order to illustrate the spectral resolution of pixilated spectrometer, the monochromatic light source centered at 650 nm is used as the incident light. The whole process of spectrum detection is shown in Fig. 1. For the monochromatic light detection, the number of driven voltage *n* is 20 with a sampling interval of 0.1 V, and the wavelength ranges from 500 to 700 nm. According to the above formula (4)–(6), the reconstructed spectrum can be obtained with the known detected intensity and transmittance matrix. Fig. 3 shows the monochromatic spectrum which is produced accurately at the peak wavelength being 650 nm. We define the full width at half maximum (FWHM) of the peak as the spectrum resolution, as a result, the resolution of reconstructed spectrum can achieve about 0.2 nm from the inserts shown in Fig. 3. Due to the sampling interval $\Delta\lambda_m$ being 0.1 nm, the value of μ_m in equation (7) can be directly calculated from the spectrum resolution. To obtain an accurate spectrum recovery with high resolution, the select of the sparse dictionary is crucial. As for a simple incident spectrum, the Gaussian function chosen as sparse dictionary $\varphi = A*\exp((m - \mu)^2/\sigma^2)$ (where $A = 1$) can be easily determined with only two parameters, the position μ and the width σ.

Furthermore, to demonstrate the spectrum recovery ability of pixilated spectrometer, bandpass light created by bandpass filter in front of continuous light is selected to carry out the measurement. This bandpass spectrum has a center wavelength at 668.8 nm with the half-width 9 nm. The process of spectrum detection is consistent with the monochromatic light detection. Fig. 4(a)–

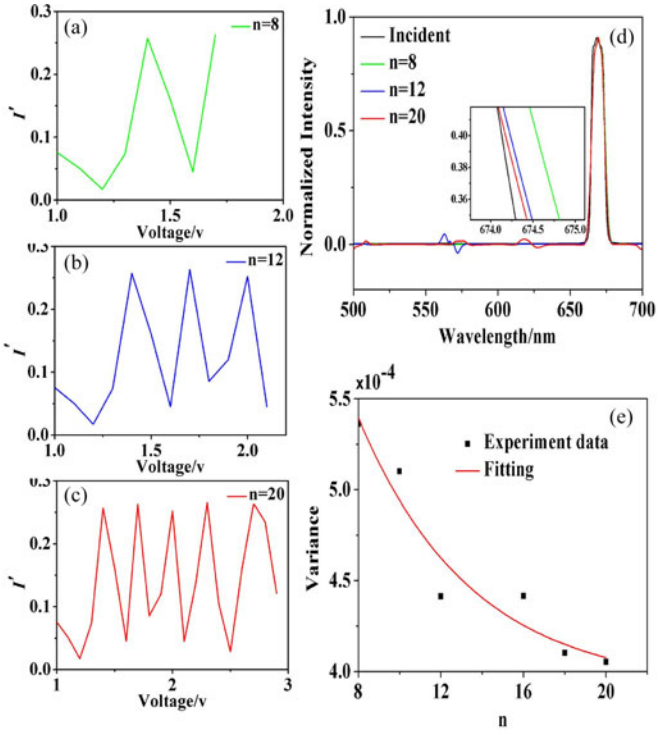

Fig. 4. (a)–(c) Detected intensity of $n = 8$, 12, and 20, respectively. (d) is reconstructed result. The green, blue, and red curves represent the reconstructed spectrum with a sampling number of 8, 12, and 20, respectively. (Inset) Magnified center wavelength. (e) is the variance between the incident and reconstructed spectrum of different value of n.

(c) shows the corresponding detected intensities under the sampling number n of the driven voltage being 8, 12, and 20, respectively. It can be found that the information of the detected intensity is more precise with the increase of sampling number n. In Fig. 4(d), the black line corresponds to target spectrum directly detected by the spectrophotometer Lambda 35, which is used as the incident spectrum in the experiment compared with the proposed spectrometer. The green, blue and red curves shown in Fig. 4(d) correspond to the reconstructed spectrum with a sampling number of 8, 12 and 20 respectively. Those spectrum curves are almost consistent with that of the incident light, which demonstrates the effectiveness of the pixilated spectrometer. With $n = 8$, the incident spectrum is produced reasonably well, whereas it suffers a severe spectral broadening at the central wavelength. When $n = 12$ and 20, the incident spectrum is produced accurately at the peak position while some side lobes exists. Since the performance of spectrum reconstruction is a trade-off between the system noise and the optical modulation ability of LC, with the increase of sampling number n, the sampling scanning speed accelerates at the same time, which results in the accumulation of the system noise and the inevitability of side lobes. On the whole, reconstructed results can be concluded that the spectrum is reconstructed more accuracy with larger sampling number, which attributes to the optical modulation ability of LC. To recover this complex spectrum in Fig. 4(d), the mixed Gaussian functions with more parameters are required. Here, the superposition of three Gaussian functions is used, $\varphi = A_1 * \exp((m - \mu_1)^2/\sigma_1^2) + A_2 * \exp((m - \mu_2)^2/\sigma_2^2) + A_3 * \exp((m - \mu_3)^2/\sigma_3^2)$, which means 9 parameters should be solved. Furthermore, the deviation between the incident and reconstructed spectrum is calculated under the condition of different values of driven voltage. The results in Fig. 4(e) show that, except for one aberrant point distributed above the curve, the variance is basically exponentially decreased with the increase of n. On the other hand, we speculate that

the variance tends to be stable with the increase of n, which reveals that the accuracy of the reconstructed spectrum cannot be infinitely improved.

The pixilated spectrometer possesses many advantages. First, the high-resolution can be achieved without sacrificing the spectral range. Another advantage of the pixilated spectrometer is its good optical modulation ability with only one liquid crystal, dispensing with designing and fabricating the complex filter array, which actually simplifies system test and measurement. Lastly, an adaptive sparse dictionary can be selected to reconstruct any complex spectrum, which can achieve high-performance spectrum reconstruction. Given the ability to make the polarizer like a thin film and post on both sides of LC, it is possible to integrate experimental devices into a chip that can apply to many fields like imaging microspectrometer or smart phone.

4. Conclusion

In this paper, the pixilated spectrometer combined single liquid crystal (LC) with a sparse algorithm is analyzed. We experimentally demonstrated the accuracy of reconstructed spectrum and high spectrum resolution. The pixilated spectrometer with small size, high-energy efficiency, and high spectrum resolution makes it a good candidate for imaging microspectrometer used in the integrated optical system.

References

[1] C. P. Bacon, Y. Mattley, and R. Defrece, "Miniature spectroscopic instrumentation: Applications to biology and chemistry," *Rev. Sci. Instrum.*, vol. 75, no. 1, pp. 1–16, 2004.
[2] J. S. Milne, J. M. Dell, A. J. Keating, and L. Faraone, "Widely tunable MEMS-based Fabry–Perot filter," *J. Microelectromech. Syst.*, vol. 18, no. 4, pp. 905–913, 2009.
[3] K. Chaganti, I. Salakhutdinov, I. Avrutsky, and G. W. Auner, "A simple miniature optical spectrometer with a planar waveguide grating coupler in combination with a plano-convex lens," *Opt. Exp.*, vol. 14, no. 9, pp. 4064–4072, 2006.
[4] Z. Xia *et al.*, "High resolution on-chip spectroscopy based on miniaturized microdonut resonators," *Opt. Exp.*, vol. 19, no. 13, pp. 12356–12364, 2011.
[5] C. C. Chang and H. N Lee, "On the estimation of target spectrum for filter-array based spectrometers," *Opt. Exp.*, vol. 16, no. 2, pp. 1056–1061, 2008.
[6] S. W. Wang, C. Xia, X. Chen, and W. Lu, "Concept of a high-resolution miniature spectrometer using an integrated filter array," *Opt. Lett.*, vol. 32, no. 6, pp. 632–634, 2007.
[7] U. Kurokawa, B. I. Choi, and C.-C. Chang, "Filter-based miniature spectrometers: Spectrum reconstruction using adaptive regularization," *IEEE Sens. J.*, vol. 11, no. 7, pp. 1556–1563, Jul. 2011.
[8] P. Wang and R. Menon, "Computational spectrometer based on a broadband diffractive optic," *Opt. Exp.*, vol. 22, no. 12, pp. 14575–14587, 2014.
[9] M. Sluijter, D. K. G. De Boer, and H. P. Urbach, "Simulations of a liquid-crystal-based electro-optical switch," *Opt. Lett.*, vol. 34, no. 1, pp. 94–96, 2009.
[10] N. Wang, G. Li, and M. Yun, "Voltage-dependent birefringence measurements of liquid crystals," *Chin. J. Lasers*, vol. 29, no. 12, pp. 1064–1066, 2002.
[11] G. J. Ren and J. Q. Yao, "Voltage-tunable liquid crystal filter," *Acta Photon. Sin.*, vol. 39, no. 5, pp. 789–791, 2010.
[12] J. Oliver, W. Lee, S. Park, and H.-N. Lee, "Improving resolution of miniature spectrometers by exploiting sparse nature of signals," *Opt. Exp.*, vol. 20, no. 3, pp. 2616–2618, 2012.
[13] O. Aharon and I. Abdulhalim, "Liquid crystal Lyot tunable filter with extended free spectral range," *Opt. Exp.*, vol. 17, no. 14, pp. 11426–11433, 2009.
[14] J. Beeckman, T. Hui, P. J. M. Vanbrabant, R. Zmijan, and K. Neyts, "Polarization selective wavelength tunable filter," *Mol. Cryst. Liquid Cryst.*, vol. 502, no. 1, pp. 19–28, 2009.
[15] B. B. Kyotoku, L. Chen, and M. Lipson, "Cavity enhanced on-chip spectrometer with sub-nm resolution," in *Proc. Conf. Lasers Electro-Optics, Opt. Soc. Amer.*, CWG5, 2010.
[16] J. Cui *et al.*, "A microspectrometer based on subwavelength metal nanohole array," *Proc. SPIE*, vol. 9272, pp. 92721O-1–92721O-5, 2014.
[17] J. Yang, J. Wright, T. S. Huang, and Y. Ma, "Image super-resolution via sparse representation," *IEEE Trans. Image Process.*, vol. 19, no. 11, pp. 2861–2873, Nov. 2010.